iScience

CellPress
OPEN ACCESS

Article

Achieving net zero energy heating by integrating the building envelope as a thermal battery

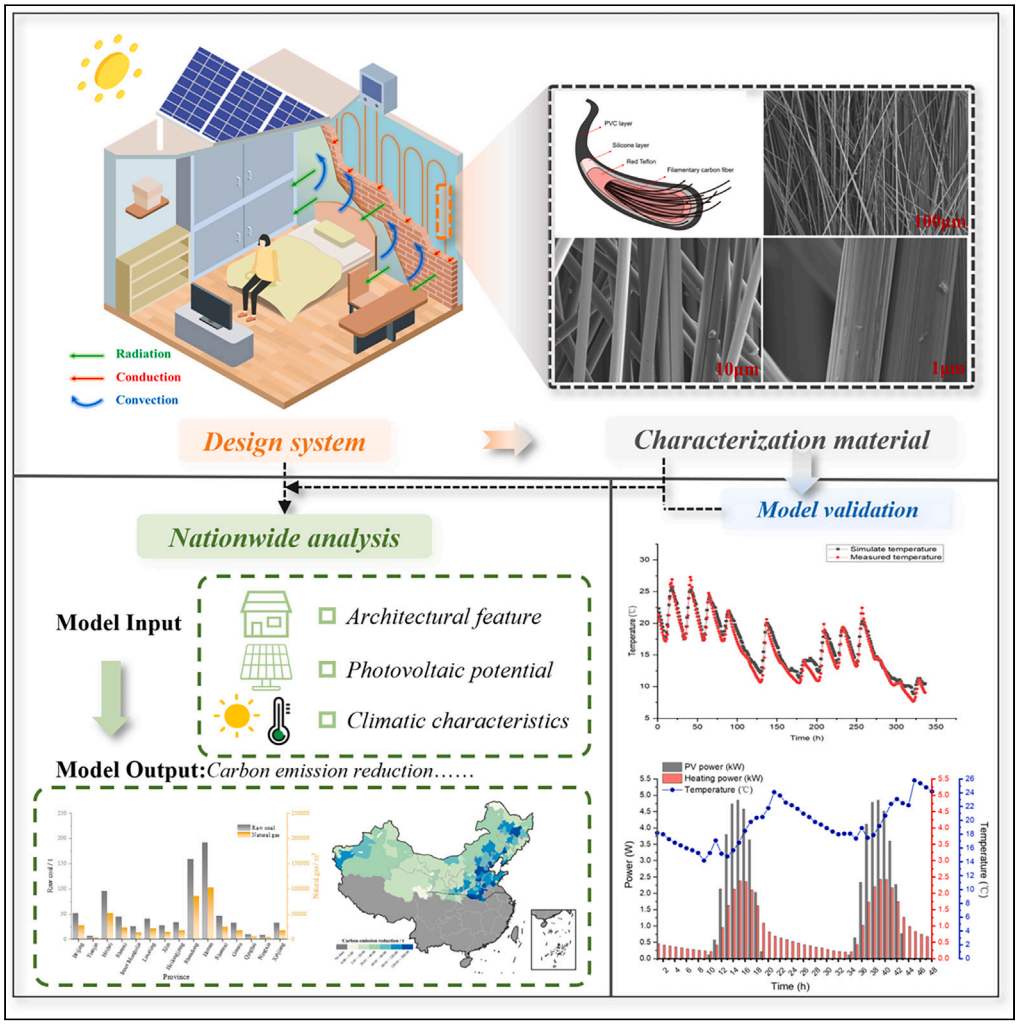

Yuan Zhi, Tao Sun, Ding Gao, Xiaomeng Chen, Guanqiong Wei, Xilei Dai, Xudong Yang

xyang@tsinghua.edu.cn

Highlights

Building envelope transforms into a thermal battery for photovoltaic heating systems

We introduced a top-down performance assessment model for envelope-embedded systems

Building envelope has a high energy storage capacity

The envelope-embedded will contribute greatly to China's carbon reduction

Zhi et al., iScience 27, 109892
June 21, 2024
https://doi.org/10.1016/j.isci.2024.109892

iScience

CellPress
OPEN ACCESS

Article

Achieving net zero energy heating by integrating the building envelope as a thermal battery

Yuan Zhi,[1] Tao Sun,[2] Ding Gao,[1] Xiaomeng Chen,[3] Guanqiong Wei,[1] Xilei Dai,[4] and Xudong Yang[1,5,6,*]

SUMMARY

Photovoltaic (PV) heating is a promising technology for achieving fossil fuel–free heating and carbon neutrality in the building sector. Cost-effective energy storage plays a critical role in PV heating to solve the temporal mismatch between supply and demand. Herein, we propose the concept of using a building envelope as an active energy-storage device for a PV heating system, thus transforming the building envelope into a thermal battery. Experimental results show that the energy storage capacity of 142 kW h/m^2, which is higher than that of conventional thermal storage systems. We developed a top-down macro performance assessment model to quantify the contribution of a PV heating system using a building envelope as energy storage. By our estimation, the envelope-embedded system can reduce heating-related CO_2 emissions by 7435.7 tons annually in northern China. Our study provides insights into innovative energy-saving building energy storage systems that can help achieve global carbon neutrality and sustainability.

INTRODUCTION

China is one of the largest carbon emitters worldwide. In China, buildings account for approximately 37% of the annual energy consumption and carbon dioxide (CO_2) emissions.[1,2] Heating systems are responsible for more than 40% of the total building energy use in northern China.[3,4] Therefore, China must take effective measures to reduce carbon emissions associated with building heating to meet its commitment to achieve carbon neutrality by 2060. Reducing the energy and fossil fuel consumption of heating systems contributes significantly to sustainable development.

Increasing the proportion of photovoltaic (PV) power in building energy systems is an effective way of achieving sustainability.[5,6] However, a deeper penetration of PV energy will only be implementable with scalable, affordable, and sustainable energy storage, owing to dramatic fluctuations in the PV power.[7–9] Therefore, tremendous efforts have been made to develop energy storage technologies, including electrochemical energy storage, phase change energy storage, flywheel energy storage, and compressed air energy storage.[10–12] However, the thermal storage capacity of building envelopes has largely been overlooked, despite the fact that the thermal energy loss of a building envelope is responsible for the majority of the total energy consumption and its thermal inertia has considerable thermal storage potential.[13,14] Therefore, it is essential to develop innovations in science and technology for converting the building envelope from an energy-consuming unit into an energy-storing unit, thereby providing a large amount of energy-storage resources for PV systems, increasing the penetration of PV power into the building energy system, and reducing the carbon footprint.

The use of electrochemical batteries for energy storage in PV systems has become one of the main options for mitigating the volatility of PV power.[15,16] However, the large battery capacity required to support the energy needs of a building leads to unaffordable costs for energy storage systems.[17] Moreover, batteries have a limited lifespan and their production and recycling processes can potentially pollute the environment.[18–20] In addition, the risk of battery explosion has not yet been completely resolved. Therefore, it is not the best option to use batteries for energy storage in building heating systems. Recent studies have proposed the incorporation of thermal storage devices into building energy systems as storage options for PV systems, such as water tanks, buried pipes, and phase change materials.[21–24] These heat storage devices are less expensive than batteries. However, the space required for these thermal storage devices is considerably larger than that available in buildings. Therefore, there is insufficient space for developing thermal storage devices for building energy systems, especially in urban buildings.[25,26] To be scalable, energy storage in building energy systems should have an affordable cost, be small, and have a long service life. A building envelope is perfectly suited to these requirements. However, the thermal storage capacities and potential contributions of building envelopes have rarely been studied.

[1]Department of Building Science, Tsinghua University, Beijing 100084, China
[2]Guangdong Construction Engineering Architectural Design Group Co., Ltd, Guangzhou 510000, China
[3]College of Information and Electrical Engineering, China Agricultural University, Beijing 100084, China
[4]School of Electrical and Electronics Engineering, Nanyang Technological University, Singapore 639798, Singapore
[5]Shanxi Research Institute for Clean Energy, Tsinghua University, Taiyuan 030032, China
[6]Lead contact
*Correspondence: xyang@tsinghua.edu.cn
https://doi.org/10.1016/j.isci.2024.109892

Previous studies have only considered the building envelope as an energy-consuming unit and regarded improving the insulation performance of the envelope as a means of saving energy.[27–30] In fact, the building envelope can be multifunctional if well explored. First, the building envelope has thermal inertia and the ability to store heat.[31] Second, the large mass of a building envelope can provide significant energy storage capacity without taking up additional space. Third, a large building envelope facilitates the creation of a uniform temperature environment as it is a radiant terminal heating unit. Most importantly, a building envelope is an almost free energy storage and heating device for the occupants.

In this study, we develop a concept that transforms building envelopes into a thermal battery to provide a solution for PV heating systems that is inexpensive and small. The system aims to transform building envelopes from an energy consumer to an energy storage provider with the goal of providing affordable and sustainable energy storage for PV systems, thereby increasing the flexibility of building energy systems and the penetration of PV power, which could accelerate the switch toward sustainable building choices.

RESULTS

Modeling and description of thermal storage system based on building envelope

Storing heat from a PV power conversion in a building envelope is a challenge. On the one hand, such a heating system places higher demands on the heating devices. Traditional heating devices such as heat pumps and electric heaters require a constant voltage for stable operation; thus, their heating power cannot match the fluctuating PV power.[31,32] Some resistive elements such as metal wires and ceramic tubes can operate with voltage fluctuations and thus receive all of the PV energy. However, it is difficult to guarantee the thermal stability and safety of these materials in high-temperature environments.[33,34] The heating devices needed for this study should be able to work at fluctuating voltages and have a heating power and surface temperature that meets the thermal comfort requirements of the occupants. Also, to store as much heat as possible in the building envelope, the heating equipment needs to be integrated into the envelope, and the envelope needs to be fitted with insulated panels to prevent heat from escaping to the outside through the building envelope, which would result in a waste of heat.[35] Therefore, the surface temperatures of the heating equipment must be strictly limited to specific ranges, and the temperatures of the envelope sections must be precisely calculated. An envelope with a low temperature results in less heat being stored, making it difficult to ensure an adequate heating performance. An envelope with a higher temperature, however, which exceeds the tolerance temperature of the insulation material, can be a safety hazard. Therefore, the challenge of this research is to store electrical energy with drastic voltage fluctuations within a building envelope through a low-cost solution that makes the building envelope a heat source with low fluctuations.

To address these challenges, we propose a PV heating system based on heat storage in a building envelope, as shown in Figure 1. The system operates as follows. PV power is fed directly into the heating equipment buried in the building envelope to heat the building walls, and the envelope then releases heat into the rooms via convection heat transfer and thermal radiation. This way, the building envelope becomes a heat storage device as well as a heating terminal equipment for the building energy system, while not taking up extra space in the building. Envelope-embedded approaches increase the thermal inertia of building envelopes, thereby reducing the temperature fluctuations and heat loss in the building envelope. In addition, this method provides a huge energy storage resource and realizes the direct use of PV power for heating, thus saving building heating energy and reducing CO_2 emissions. The innovation of this research is the use of low-cost materials and a simple system structure that replace previous complex and expensive energy storage solutions. To realize the above system design, a novel heating device that cannot only operate under conditions of fluctuating voltage and power but can also easily be integrated into the envelope and is thermally stable in various environments is developed, as detailed below.

To quantify the performance of a PV heating system using a building envelope as energy storage and its contribution to reducing heating-related carbon emissions in China, we developed a top-down macro performance assessment model. Although some commercial energy simulation software, such as EnergyPlus and DeST, can calculate the heating energy consumption and indoor temperature of a building, they are unable to model heating terminals with such a special structure and describe such specific heat transfer processes.[36–38] Meanwhile, previous data-driven PV power models seldom considered the effects of MPPT algorithms or incorporated weather conditions, geographic location, and installation conditions, and are therefore not universally applicable.[39] More importantly, no studies have quantitatively characterized the contribution of PV heating systems to CO_2 emission reduction in China. Considering these requirements, we introduce a detailed performance assessment model for a PV heating system based on envelope-based thermal storage.

The assessment model was divided into five parts, as illustrated in Figure 1B. First, we established a PV power model considering meteorological parameters, PV installation conditions, and the MPPT algorithm to obtain the hourly power supply to the heating system. It is considered as a charging power model for a thermal battery. Second, the heating load of the building was calculated using a difference method based on MATLAB and DeST. It is considered to be an exothermic model of a thermal battery. Third, the power supply for PV heating was combined with the building load to obtain the indoor temperature of the building and a reasonable system capacity. Fourth, we used a modified U-net semantic segmentation model based on satellite images to obtain the potential of rooftop PV systems in rural buildings across the country and combined the results with the model in the third step to obtain the sizes of PV heating systems in the northern provinces of China. Finally, the CO_2 emission reduction contribution of PV heating systems to each province was obtained based on the carbon emission factor method. The detailed modeling procedure is shown in the supplemental information.

Heating device and its characteristics

We adopted the strategy of using carbon fiber as the main material for the heating devices to achieve the desired properties. The construction of a carbon-fiber electric heating wire is shown in Figure 2A. The innermost part of the electric heating wire is a filamentary carbon fiber, which

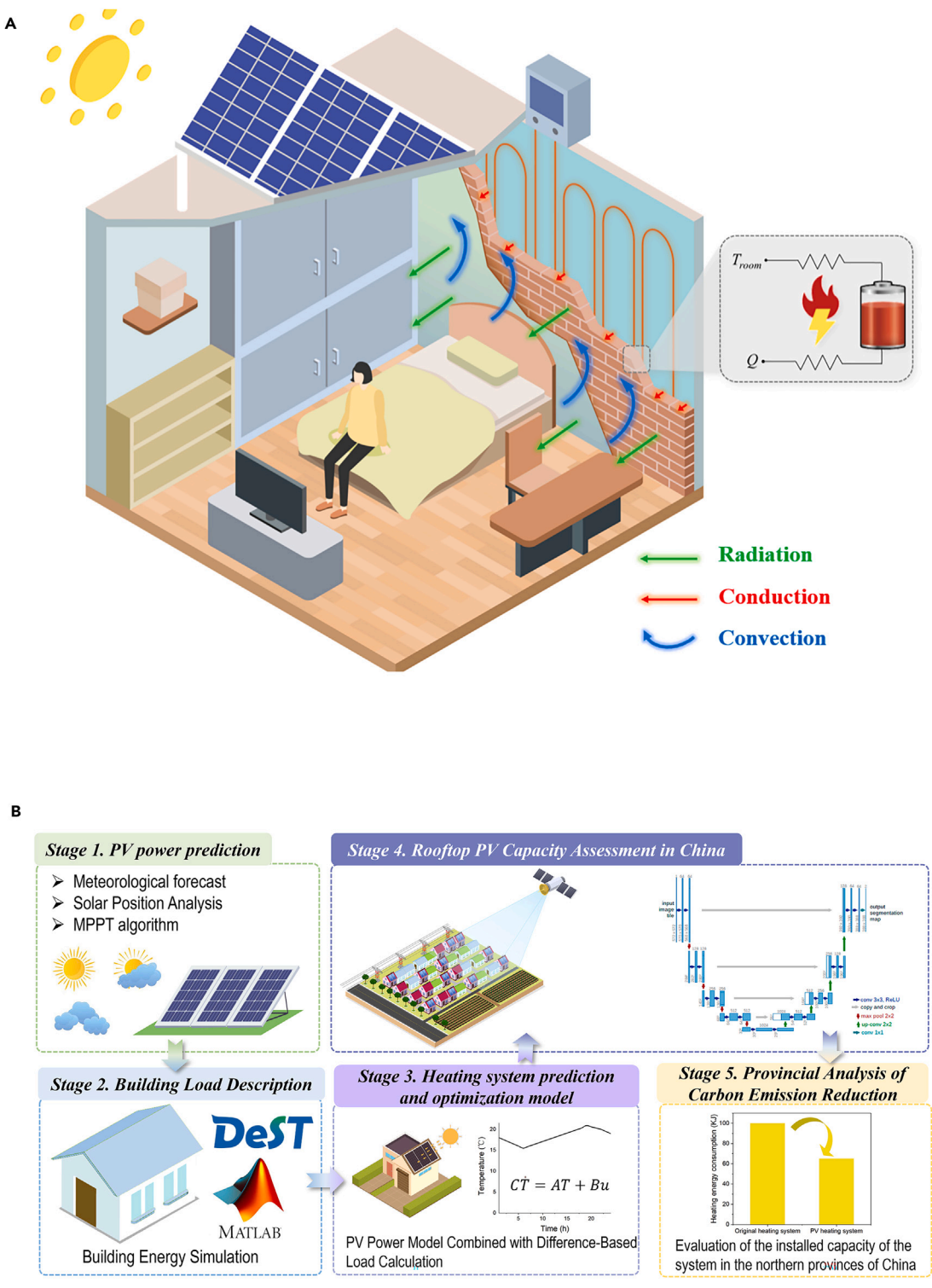

Figure 1. Photovoltaic heating system based on heat storage in the building envelope

(A) System Schematic.

(B) Model flowchart.

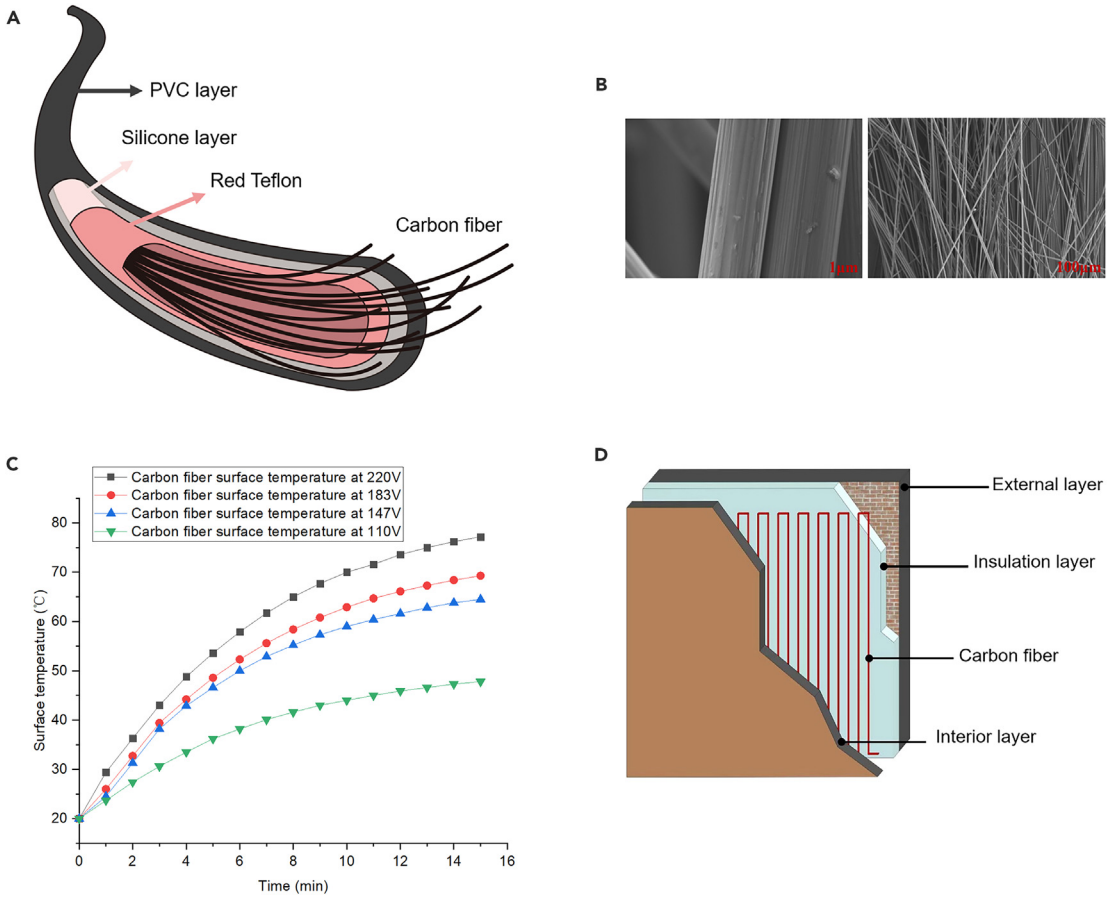

Figure 2. Material and structural analysis of building envelopes

(A) Structure of carbon fiber electric heating wire. Carbon fiber electric heating wire combines flexibility and high thermal conductivity.

(B) SEM of the carbon fiber. The magnifications from left to right are 100×, 1000x, and 5200x in that order. The rough surface of the column facilitates heat transfer.

(C) Test results of electric heating wire surface temperature at different voltages. The surface of the carbon fiber heating wire heats up quickly and the surface temperature does not damage the insulation material.

(D) Structure of system based on heat storage in the building envelope.

is the core heating component of the wire. The outer side of the carbon-fiber wire is wrapped in red Teflon, silicone, and PVC layers. These wrapping layers are soft, making it possible to bend them into any shape for easy integration into the enclosure. SEM images of the carbon fiber filaments at 100x and 5000× magnification in SEM are shown in Figure 2B. The carbon fibers used in this study were straight and slim filaments with vertical stripes on their surfaces, which increased the heat transfer area and facilitated heat transfer.[40] Changes in the surface temperature of the electric heating wire at different voltages are shown in Figure 2C. The higher the temperature, the faster the surface temperature of the electric heating wire increases, and the higher the final equilibrium temperature increases. The surface equilibrium temperature of the electric heating wire at 220 V is below 80°C. This temperature does not damage the insulation board, bricks, or other building materials.[41,42] Therefore, the combination of a carbon fiber electric heating wire and the building envelope does not damage the thermal insulation or structural performance of the building envelope.

The structure of the carbon-fiber electric wire integrated into the building envelope is illustrated in Figure 2D. Figure 2D shows the system as a whole fastened to the interior surface of the building's original envelope. Along the cross-section, going from indoor to outdoor, is as follows: heat storage wall, carbon fiber electric wire, insulation board, and building exterior wall. The function of the insulation board is to prevent heat from being transferred to the outdoors, while reducing the heating load of the building. The carbon fiber electric heating wire was connected to the PV electricity to generate heat, which was then stored in the heat storage wall by means of heat conduction. The heat storage wall supplied heat to the room via convective heat transfer and radiation. Consequently, the building envelope was transformed from an energy-consuming unit into a component that integrates insulation, heat storage, and heating. The building envelope performs the functions of insulation panels, thermal batteries, and terminal heating equipment.

Compared to conventional commercial heating equipment, for example heat pumps, although heat pumps offer higher energy efficiency ratios, they require a stable voltage and energy supply to operate, thus increasing the cost of the control system and energy conversion losses.

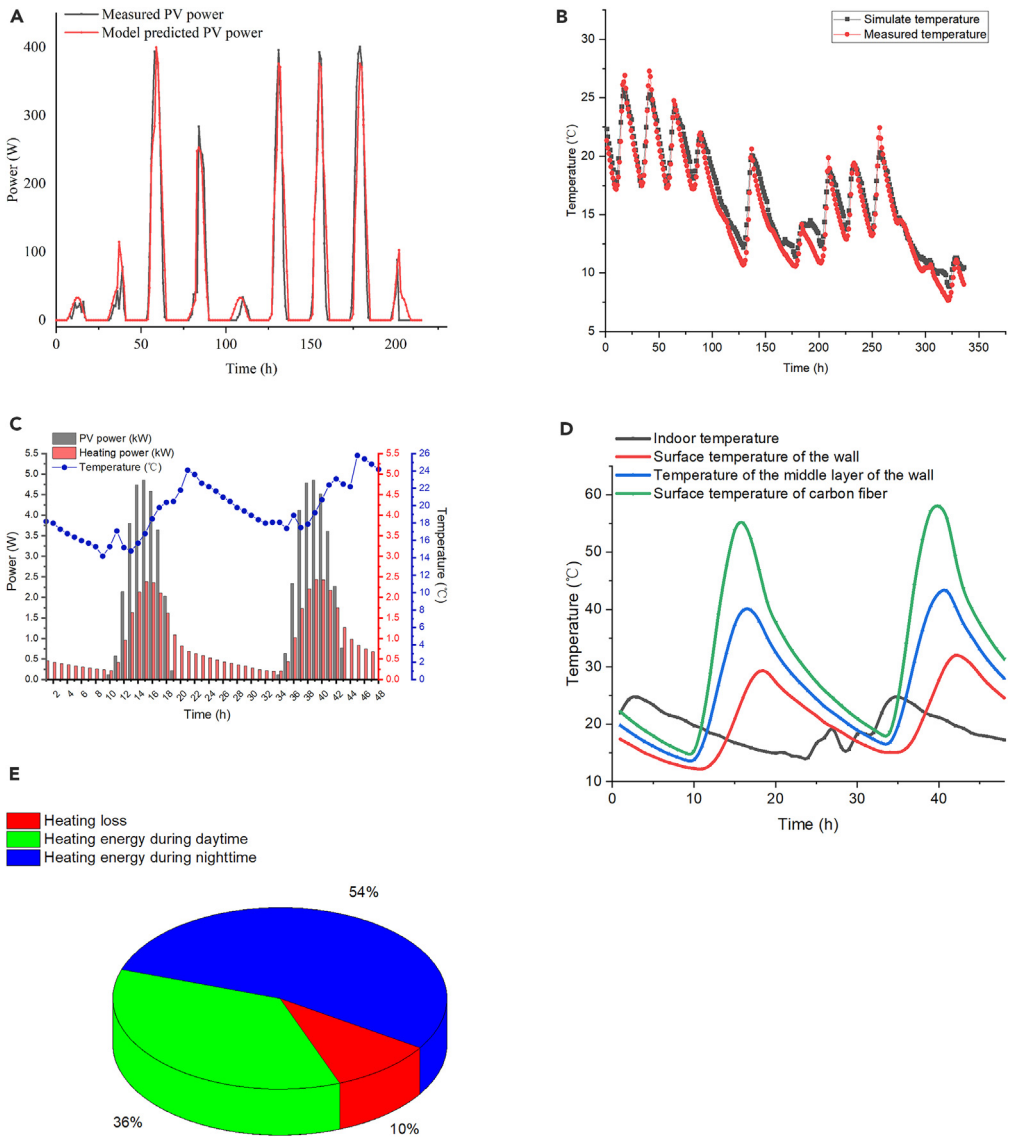

Figure 3. Test results of a photovoltaic heating system based on heat storage in the building envelope

(A) Verification of the accuracy of a thermal battery charging model. The relative error is within 10%.

(B) Validation of the accuracy of exothermic modeling of thermal batteries. Relative error is within 1.5°C.

(C) Performance of heating based on heat storage in the building envelope. The indoor temperature can satisfy people's thermal comfort at any given moment.

(D) Test results for the temperature of different cross sections of the thermal storage wall and the indoor air temperature. The building envelope effectively reduces fluctuations in temperature due to fluctuations in PV power.

(E) Heat balance results of the heating system. Heat storage in the envelope releases about 60% of the heating energy at night.

Whereas, the heating device proposed in this study can be used for fluctuating voltage and power supply scenarios, thus saving the cost of the control system and reducing the energy conversion losses to achieve one hundred percent self-consumption of PV power.

Thermal effect demonstration

To verify the effectiveness of the heating system and the accuracy of the model, we installed the system in a farmhouse and tested it in the field. As a pilot demonstration, the above device was installed for heating in a 15 m^2 room in Ruicheng (North latitude 34°36′-48,′ East longitude 110°36′-42′), in northern China. We compare the test results with the model predicted values as shown in Figures 3A and 3B. After a week of testing under different weather conditions, the PV power model, i.e., the thermal battery charging model, predicted results within 10% relative error to the measured data as shown in Figure 3A. The maximum difference between the indoor temperature predicted by the thermal battery exothermic model and the measured indoor temperature for 2 consecutive weeks did not exceed 1.5°C, as shown in Figure 3B. The

Table 1. Performance comparison of thermal batteries with other commercial energy storage

Performance indicators	Li-ion battery	Flow battery	Pumped storage	Compressed air energy storage	Thermal battery
Cycle life/times	6000	15000	–	–	–
System life/year	12	30	50	30	70
Power cost/yuan/kW	300	1746	5000	8000	125
Capacity cost/yuan/kW·h	800	863	100	100	12

model predictions match the measured results, indicating that the model has high accuracy. The PV power, room temperature, and the temperatures at different locations in the wall cross-section were measured throughout the heating season. Figure 3C illustrates the experimental results for typical sunny days. It can be seen that the fluctuations in the heating power supplied by the building envelope to the room are significantly smaller than the fluctuations in the PV power. Even at night, when there was no PV power, the heat stored in the building envelope was released into the rooms to maintain heating. Because our proposed heating method based on heat storage in the building envelope mainly supplies heat to the room through thermal radiation, the dry-bulb temperature of the indoor air is not representative of the thermal sensation the occupants experience.[43] Therefore, we used the average radiation temperature, which considers thermal radiation, for estimating the heating performance. The expression for the average radiation temperature is shown in Equation 1.[44]

$$t_r = t_g + 2.37\sqrt{v}\left(t_g - t_a\right) \quad \text{(Equation 1)}$$

Where t_r is the average radiation temperature, °C; t_g is the black-bulb temperature, °C; t_a is the air temperature, °C; v is the wind speed, m/s. The average radiant temperature takes into account the combined effect of convection and radiation on the thermal sensation of the human body and is suitable for evaluating the thermal comfort of the human body. The energy supply characteristics and indoor black bulge temperature of the PV heating system after adoption of the building envelope as heat storage device are shown in Figure 3C for an average outdoor temperature of −3°C. As the envelope can heat the room by releasing its own stored heat during the night when there is no PV power input, the indoor black-bulb temperature can be maintained at above 14°C even during the night. The heat storage in the envelope makes the heating power flatter and time-delayed compared with the PV power, so that the indoor black-bulb temperature peaks at around 7 p.m. at around 26°C. This prevents overheating in the afternoon when the sun is at its strongest. Therefore, PV-carbon fiber heating based on thermal storage in the envelope can meet the heating needs of occupants while avoiding the challenges of cold nights and hot afternoons.

Figure 3D compares the results of the temperature sensors in the envelope at different locations in the thickness direction, and shows that the heat storage of the building envelope effectively mitigates the temperature fluctuations caused by fluctuations in the heating power. The fluctuations gradually decreased from the surface temperature of the carbon-fiber hot wire to the air temperature of the indoor room. Because of the heat storage effect of the envelope, fluctuations in the indoor air temperature were reduced to a quarter of the fluctuations in the surface temperature of the electric heating wire. The heat storage of the building envelope connects the fluctuating power supply to a stable heat load.

Simultaneously, according to the monitoring temperatures of different cross-sections of the building envelope combined with the differential method (Section 2 in the supplemental information), we can obtain the heat balance results of the heating system, as shown in Figure 3E. Ten% of the heat generated by the carbon fiber was transferred to the outdoor environment, which was the heat loss of the heating system, and the remaining 90% of the heat was transferred indoors to heat the room. 60% of the heating power is released from the building envelope to the interior during the night when no PV power is available, indicating that the thermal storage of the envelope makes an important contribution to mitigating the fluctuations in the PV heating power. The heating energy released from the building envelope to the rooms during the whole heating season is 2130.9 kW h, which is 93.6% of the heat stored in the envelope. Table 1 compares the performance of thermal batteries with that of conventional commercial energy storage devices, which can achieve higher energy performance while significantly reducing costs. Throughout the heating season, the building envelope was used as a thermal battery to provide an energy storage capacity of 142 kWh per square meter, with an average heat release intensity of 49.4 W/m^2.

Thermal modeling and energy-saving evaluation

The heating energy savings and CO_2 reductions achieved by envelope-embedded systems must be calculated in relation to the PV potential and building load. We developed a thermal model (see supplemental information and Supplementary equations, pages 9–17 and Table S1 for more details) for quantifying the energy savings from building heating through envelope-embedded PV heating approaches. The model calculates the potential thermal storage capacity of building envelopes adapted to PV systems in different cities in northern China while comparing the reductions in the building thermal load and CO_2 emissions. Based on the roof area identified by satellite imagery for each province in northern China (see Figure S6 in the supplemental information), the installed rooftop PV potential for each city in the northern provinces as well as the heating area for which it can be adapted can be calculated. The baseline is the building energy use under the existing building envelope with the most common radiators for heating. The savings in coal consumption are calculated based on a timescale of the entire heating season, where the energy for heating comes entirely from PV and the indoor temperature is maintained at 14°C or higher. The coal and natural gas savings from envelope-embedded PV heating for each province are shown in Figure 4A, and can lead to a total of 11098.1

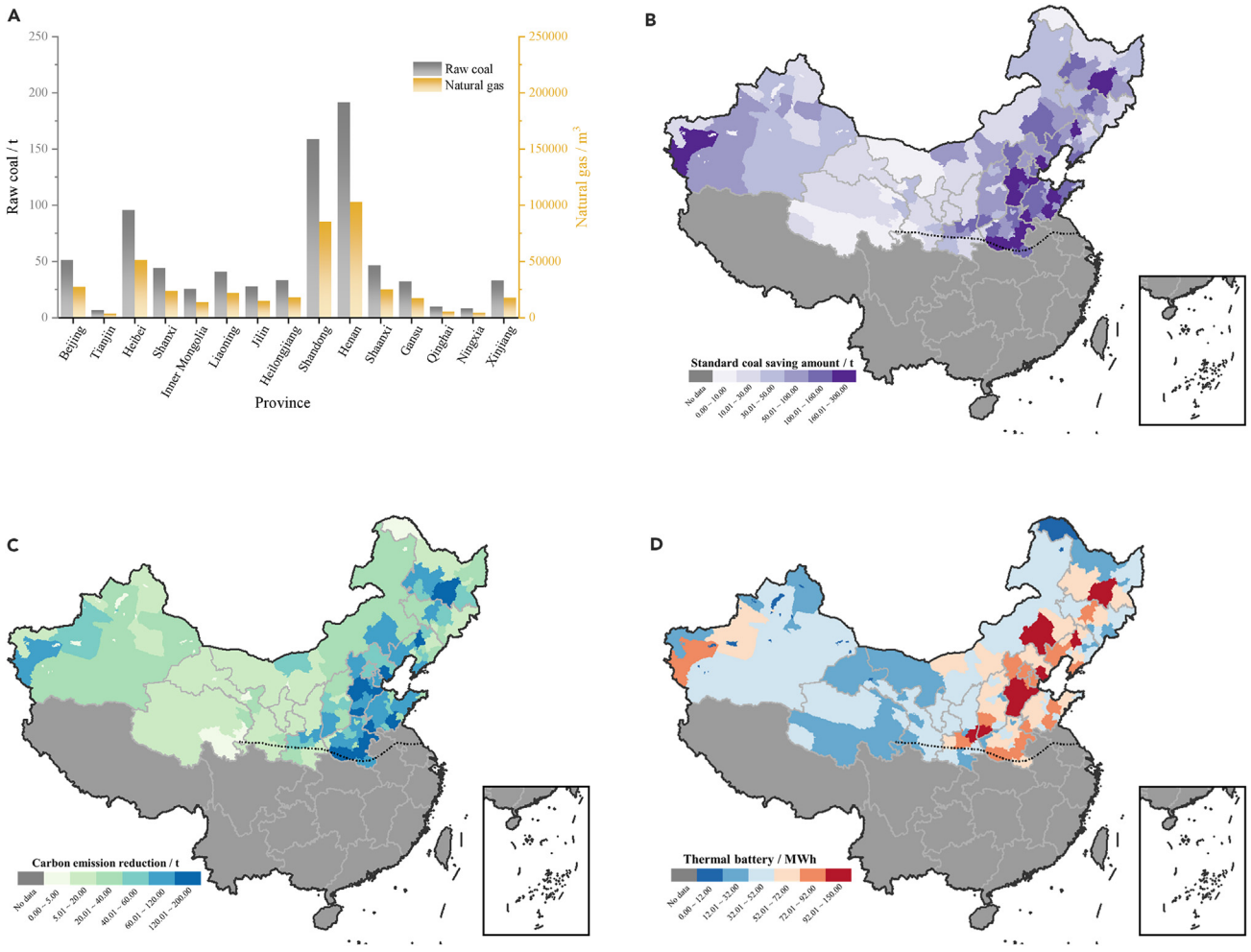

Figure 4. The benefits of converting buildings into thermal batteries

Since the building envelope becomes a free energy storage for the PV heating system, the increase in storage capacity leads to an increase in PV penetration and a decrease in fossil energy consumption for building heating.

(A) Reduction in fossil energy use for building heating in different provinces.

(B) Energy savings from heating buildings in different provinces.

(C) CO_2 emission savings from heating buildings in different provinces.

(D) The capacity of the thermal battery provided by a building in different provinces. The capacity of the storage is calculated based on the theoretical range of temperature variations of the building envelope.

tons of standard coal per year in savings. The heating energy savings and CO_2 reductions resulting from the extension of this PV heating method to every northern Chinese city are shown in Figures 4B and 4C. Owing to the large building density and roof area in North and Northeast China, a greater installed PV potential leads to greater heating energy savings and CO_2 reductions.[44] It is worth mentioning that the envelope-embedded PV heating system turns the building into a thermal battery. Based on the heat storage capacity of the building envelope calculated by the model, the thermal battery capacity provided by a building with the envelope-embedded system in northern China was calculated, as shown in Figure 4D. The thermal battery capacity is based on an average of the heat released during periods without PV power throughout the heating season. According to a rough estimation, buildings in the northern provinces of China could provide 8465.1 MWh in thermal battery capacity and a national CO_2 emission reduction of 7435.7 tons annually could be achieved.

Implications

Carbon emissions from the building operation account for about 22% of all carbon emissions in China, and building heating is the main source of carbon emissions from building operations. Therefore, adopting PV power to meet building heating needs is an effective way to reduce carbon emissions in China. Conventional commercial heating devices like heat pump cannot be directly connected to PV because PV power is

fluctuating, the original system requires batteries to ensure that the system voltage is stabilized. Whereas, the system proposed in this study does not require expensive battery and control system, which is economically more promising in practical applications. The innovation of this study is to propose a performance model of a PV heating system based on thermal storage in the building envelope, as well as the concept and application of transforming the building envelope into a thermal battery. Our proposed envelope-based thermal storage approach can reduce the cost of storage for PV heating and increase the penetration of renewable energy in building heating energy systems. Figure 2D proposes a new design scheme for the envelope to take on the multiple functions of heat storage-insulation-heating.

DISCUSSION

To provide an affordable, sustainable, and scalable energy storage option for building energy savings, we developed a PV heating system based on thermal storage in the building envelope, which transforms the building envelope from an energy consumer to an energy storage component. To implement the envelope-embedded system, a carbon-fiber heating device was designed and integrated into the building envelope. Our proposed heating system and energy storage method can adapt to fluctuating PV energy by connecting directly to PV, overcoming the limitations of conventional heating devices that require stable voltage and power. The results of our experiments show that the impact of the volatility of the PV power at room temperature can be effectively mitigated by the thermal energy storage of the envelope. The building envelope thermal storage functions as a bridge to connect the fluctuating energy supply to a stable thermal load. In this study, the building envelope is transformed into a thermal battery for the heating system.

Our simulation verified the effects of heat storage in the building envelope and evaluated the energy-saving and CO_2 reduction performance of installing the envelope-embedded system. Our assessment models can be applied to buildings and climatic zones in different countries. With proper parameter design, the envelope-embedded system and carbon fiber heating equipment provide a flexible solution for both existing and new buildings to reduce the cost and space of energy storage devices for PV heating systems and achieve building heating energy savings, while satisfying the necessary comfort demands. A building envelope in northern China can provide a large energy storage capacity, as shown in Figure 4D, whereas the cost of constructing a chemical battery with the same storage capacity is more than 400 times that of using the building envelope for thermal storage. During the non-heating season, the PV power can be fed into the grid to provide zero-carbon electricity for satisfying loads around the building. We believe that the envelope-embedded system is promising for energy-efficient building applications and can contribute positively to global carbon neutrality and sustainability.

Limitations of the study

There are some limitations of this study that need to be explored in subsequent studies. On the one hand, since the energy consumption of a building is mainly related to the floor area (i.e., the roof area identified in this paper through satellite imagery), the building envelope, and local meteorological parameters. Therefore, we mainly considered these three indicators in our large-scale modeling analysis. Other factors, like variations in building topologies, also affect building loads. Since these parameters have a relatively small degree of influence and would greatly increase the complexity of the model, they were purposely simplified. On the other hand, our proposed PV heating system can achieve zero-carbon heating in single buildings (e.g., most rural buildings in China) because of the ample roof area available, high PV potential, and relatively low total heating load. However, large commercial buildings and multi-story buildings with high loads and small roof areas with low PV potentials cannot meet the building's heating needs with PV energy alone, in which case they need to be supplemented by municipal grids or other energy sources.

STAR★METHODS

Detailed methods are provided in the online version of this paper and include the following:

- KEY RESOURCES TABLE
- RESOURCE AVAILABILITY
  - Lead contact
  - Materials availability
  - Data and code availability
- EXPERIMENTAL MODEL AND STUDY PARTICIPANT DETAILS
  - Thermal battery charging model
  - Exothermic modeling of the thermal battery
  - U-net convolutional neural network model
- METHOD DETAILS
  - Material characterization
  - Thermal measurements

SUPPLEMENTAL INFORMATION

Supplemental information can be found online at https://doi.org/10.1016/j.isci.2024.109892.

ACKNOWLEDGMENTS

This study was supported by the National Natural Science Foundation of China (Grant No. 51838007), the Beijing Key Laboratory of Indoor Air Quality Evaluation and Control, the Key Laboratory of Eco Planning & Green Building (Tsinghua University), and the Ministry of Education of China.

AUTHOR CONTRIBUTIONS

Z.Y. and Y.X.D. conceived the study. Z.Y. and S.T. designed the experiments and performed material preparation and characterization with the help of D.X.L and W.G.Q., Z.Y., and G.D. performed the modeling work. G.D. and C.X.M. provided helpful discussions on DeST. Z.Y. helped to write the manuscript. Y.X.D. supervised the study. All authors provided discussion and comments.

DECLARATION OF INTERESTS

The authors declare no competing interests.

Received: March 8, 2024
Revised: April 10, 2024
Accepted: May 1, 2024
Published: May 4, 2024

REFERENCES

1. Ravindra, K., Kaur-Sidhu, M., and Mor, S. (2021). Transition to clean household energy through an application of integrated model: Ensuring sustainability for better health, climate and environment. Sci. Total Environ. *775*, 145657. https://doi.org/10.1016/j.scitotenv.2021.145657.
2. Wang, H., Liu, B., Yang, F., and Liu, F. (2021). Test investigation of operation performance of novel split-type ground source heat pump systems for clean heating of rural households in North China. Renew. Energy *163*, 188–197. https://doi.org/10.1016/j.renene.2020.08.147.
3. Gu, Y., Xu, H., Feng, R., Cheng, Y., Han, B., Ho, K.F., Wang, Z., He, Y., Qu, L., Ho, S.S.H., et al. (2023). Associations of personal exposure to domestic heating and cooking fuel emissions and epidemiological effects on rural residents in the Fenwei Plain, China. Sci. Total Environ. *856*, 159217. https://doi.org/10.1016/j.scitotenv.2022.159217.
4. National Bureau of Statistics: Consultation open. http://www.stats.gov.cn/search/s?qt=%E4%BE%9B%E6%9A%96.
5. Chen, X., Liu, Y., Wang, Q., Lv, J., Wen, J., Chen, X., Kang, C., Cheng, S., and McElroy, M.B. (2021). Pathway toward carbon-neutral electrical systems in China by mid-century with negative CO abatement costs informed by high-resolution modeling. Joule *5*, 2715–2741. https://doi.org/10.1016/j.joule.2021.10.006.
6. Joshi, S., Mittal, S., Holloway, P., Shukla, P.R., Ó Gallachóir, B., and Glynn, J. (2021). High resolution global spatiotemporal assessment of rooftop solar photovoltaics potential for renewable electricity generation. Nat. Commun. *12*, 5738. https://doi.org/10.1038/s41467-021-25720-2.
7. He, G., Michalek, J., Kar, S., Chen, Q., Zhang, D., and Whitacre, J.F. (2021). Utility-Scale Portable Energy Storage Systems. Joule *5*, 379–392. https://doi.org/10.1016/j.joule.2020.12.005.
8. Langevin, J., Harris, C.B., Satre-Meloy, A., Chandra-Putra, H., Speake, A., Present, E., Adhikari, R., Wilson, E.J., and Satchwell, A.J. (2021). US building energy efficiency and flexibility as an electric grid resource. Joule *5*, 2102–2128. https://doi.org/10.1016/j.joule.2021.06.002.
9. Moraski, J.W., Popovich, N.D., and Phadke, A.A. (2023). Leveraging rail-based mobile energy storage to increase grid reliability in the face of climate uncertainty. Nat. Energy *8*, 736–746. https://doi.org/10.1038/s41560-023-01276-x.
10. Moraski, J., and Phadke, A. (2023). Rail-based mobile energy storage as a grid-reliability solution for climate extremes. Nat. Energy *8*, 653–654. https://doi.org/10.1038/s41560-023-01284-x.
11. Ruhnau, O., Stiewe, C., Muessel, J., and Hirth, L. (2023). Natural gas savings in Germany during the 2022 energy crisis. Nat. Energy *8*, 621–628. https://doi.org/10.1038/s41560-023-01260-5.
12. Debanjan, M., and Karuna, K. (2022). An Overview of Renewable Energy Scenario in India and its Impact on Grid Inertia and Frequency Response. Renew. Sustain. Energy Rev. *168*, 112842. https://doi.org/10.1016/j.rser.2022.112842.
13. Khan, S.U., Khan, N., Ullah, F.U.M., Kim, M.J., Lee, M.Y., and Baik, S.W. (2023). Towards intelligent building energy management: AI-based framework for power consumption and generation forecasting. Energy Build. *279*, 112705. https://doi.org/10.1016/j.enbuild.2022.112705.
14. Odukomaiya, A., Woods, J., James, N., Kaur, S., Gluesenkamp, K.R., Kumar, N., Mumme, S., Jackson, R., and Prasher, R. (2022). Addressing energy storage needs at lower cost on-site thermal energy storage in buildings (vol 14, pg 5315, 2021). Energy Environ. Sci. *15*, 395. https://doi.org/10.1039/d1ee90067f.
15. Ouchi, T., Kim, H., Spatocco, B.L., and Sadoway, D.R. (2016). Calcium-based multi-element chemistry for grid-scale electrochemical energy storage. Nat. Commun. *7*, 10999. https://doi.org/10.1038/ncomms10999.
16. Pasta, M., Wessells, C.D., Huggins, R.A., and Cui, Y. (2012). A high-rate and long cycle life aqueous electrolyte battery for grid-scale energy storage. Nat. Commun. *3*, 1149. https://doi.org/10.1038/ncomms2139.
17. Zou, B., Peng, J., Li, S., Li, Y., Yan, J., and Yang, H. (2022). Comparative study of the dynamic programming-based and rule-based operation strategies for grid-connected PV-battery systems of office buildings. Appl. Energy *305*, 117875. https://doi.org/10.1016/j.apenergy.2021.117875.
18. Xia, Y., Cao, H., Xu, F., Chen, Y., Xia, Y., Zhang, D., Dai, L., Qu, K., Lian, C., Huang, K., et al. (2022). Polymeric membranes with aligned zeolite nanosheets for sustainable energy storage. Nat. Sustain. *5*, 1080–1091. https://doi.org/10.1038/s41893-022-00974-w.
19. Li, B., Liu, Z., Wu, Y., Wang, P., Liu, R., and Zhang, L. (2023). Review on photovoltaic with battery energy storage system for power supply to buildings: Challenges and opportunities. J. Energy Storage *61*, 106763. https://doi.org/10.1016/j.est.2023.106763.
20. Ma, J., and Yuan, X. (2023). Techno-economic optimization of hybrid solar system with energy storage for increasing the energy independence in green buildings. J. Energy Storage *61*, 106642. https://doi.org/10.1016/j.est.2023.106642.
21. Zhang, Y.F., Tang, J.B., Chen, J.L., Zhang, Y.H., Chen, X.X., Ding, M., Zhou, W.J., Xu, X.J., Liu, H., and Xue, G.B. (2023). Accelerating the solar-thermal energy storage via inner-light supplying with optical waveguide. Nat. Commun. *14*, 3456. https://doi.org/10.1038/s41467-023-39190-1.
22. Yao, J., Liu, W., Zhang, L., Tian, B., Dai, Y., and Huang, M. (2020). Performance analysis of a residential heating system using borehole heat exchanger coupled with solar assisted PV/T heat pump. Renew. Energy *160*, 160–175. https://doi.org/10.1016/j.renene.2020.06.101.
23. Wang, L., Guo, L., Ren, J., and Kong, X. (2022). Using of heat thermal storage of PCM and solar energy for distributed clean building heating: A multi-level scale-up research. Appl. Energy *321*, 119345. https://doi.org/10.1016/j.apenergy.2022.119345.
24. Liu, Y., Zhao, Y., Chen, Y., Wang, D., Li, Y., and Yuan, X. (2022). Design optimization of the solar heating system for office buildings based on life cycle cost in Qinghai-Tibet

plateau of China. Energy *246*, 123288. https://doi.org/10.1016/j.energy.2022.123288.
25. Guo, M., Liu, Y., Chen, Y., Gao, W., Wang, D., Tang, H., and Liu, H. (2022). Study on the effect of different types and distribution ratio of heat users on operation performance of the distributed solar centralized heating system. Energy Build. *270*, 112265. https://doi.org/10.1016/j.enbuild.2022.112265.
26. Navakrishnan, S., Vengadesan, E., Senthil, R., and Dhanalakshmi, S. (2021). An experimental study on simultaneous electricity and heat production from solar PV with thermal energy storage. Energy Convers. Manag. *245*, 114614. https://doi.org/10.1016/j.enconman.2021.114614.
27. Zhou, J., Peng, Y., Xu, J., Wu, Y., Huang, Z., Xiao, X., and Cui, Y. (2022). Vacuum insulation arrays as damage-resilient thermal superinsulation materials for energy saving. Joule *6*, 2358–2371. https://doi.org/10.1016/j.joule.2022.07.015.
28. Zhao, X., Liu, Y., Zhao, L., Yazdkhasti, A., Mao, Y., Siciliano, A.P., Dai, J., Jing, S., Xie, H., Li, Z., et al. (2023). A scalable high-porosity wood for sound absorption and thermal insulation. Nat. Sustain. *6*, 306–315. https://doi.org/10.1038/s41893-022-01035-y.
29. Peng, Y., Fan, L., Jin, W., Ye, Y., Huang, Z., Zhai, S., Luo, X., Ma, Y., Tang, J., Zhou, J., et al. (2021). Coloured low-emissivity films for building envelopes for year-round energy savings. Nat. Sustain. *5*, 339–347. https://doi.org/10.1038/s41893-021-00836-x.
30. Sandak, A. (2023). Engineered living materials for sustainable and resilient architecture. Nat. Rev. Mater. *8*, 357–359. https://doi.org/10.1038/s41578-023-00554-0.
31. Abraham, E., Cherpak, V., Senyuk, B., ten Hove, J.B., Lee, T., Liu, Q., and Smalyukh, I.I. (2023). Highly transparent silanized cellulose aerogels for boosting energy efficiency of glazing in buildings. Nat. Energy *8*, 381–396. https://doi.org/10.1038/s41560-023-01226-7.
32. Waite, M., and Modi, V. (2020). Electricity Load Implications of Space Heating Decarbonization Pathways. Joule *4*, 376–394. https://doi.org/10.1016/j.joule.2019.11.011.
33. Gilbert, T., Menon, A.K., Dames, C., and Prasher, R. (2023). Heat source and application-dependent levelized cost of decarbonized heat. Joule *7*, 128–149. https://doi.org/10.1016/j.joule.2022.11.006.
34. He, Z., Farooq, A.S., Guo, W., and Zhang, P. (2022). Optimization of the solar space heating system with thermal energy storage using data-driven approach. Renew. Energy *190*, 764–776. https://doi.org/10.1016/j.renene.2022.03.088.
35. Han, M.-E., Alston, M., and Gillott, M. (2022). A multi-vector community energy system integrating a heating network, electricity grid and PV production to manage an electrified community. Energy Build. *266*, 112105. https://doi.org/10.1016/j.enbuild.2022.112105.
36. Wang, R., Zhu, Y., Fu, J., Yang, M., Ran, Z., Li, J., Li, M., Hu, J., He, J., and Li, Q. (2023). Designing tailored combinations of structural units in polymer dielectrics for high-temperature capacitive energy storage. Nat. Commun. *14*, 2406. https://doi.org/10.1038/s41467-023-38145-w.
37. Kayo, C., Sanjo, K., Sato, I., Liu, M., Prasetyadi, G.V., and Hirahara, S. (2023). Carbon stocks of particle board and fiberboard in Japan. Sci. Rep. *13*, 9846. https://doi.org/10.1038/s41598-023-37132-x.
38. Zhi, Y., Sun, T., and Yang, X. (2023). A physical model with meteorological forecasting for hourly rooftop photovoltaic power prediction. J. Build. Eng. *75*, 106997. https://doi.org/10.1016/j.jobe.2023.106997.
39. Raman, G., Raman, G., and Peng, J.C.H. (2022). Resilience of urban public electric vehicle charging infrastructure to flooding. Nat. Commun. *13*, 3213. https://doi.org/10.1038/s41467-022-30848-w.
40. Xiong, J., Guo, S., Wu, Y., Yan, D., Xiao, C., and Lu, X. (2023). Predicting the response of heating and cooling demands of residential buildings with various thermal performances in China to climate change. Energy *269*, 126789. https://doi.org/10.1016/j.energy.2023.126789.
41. Jiang, Q., Li, Q., Zhang, C., Wang, J., Dou, Z., Chen, A., Yang, Y., Ren, H., and Zhang, L. (2023). Excavation of building energy conservation in university based on energy use behavior analysis. Energy Build. *280*, 112726. https://doi.org/10.1016/j.enbuild.2022.112726.
42. Sun, T., Shan, M., Rong, X., and Yang, X. (2022). Estimating the spatial distribution of solar photovoltaic power generation potential on different types of rural rooftops using a deep learning network applied to satellite images. Appl. Energy *315*, 119025. https://doi.org/10.1016/j.apenergy.2022.119025.
43. Yang, L., Wang, F., Zhao, S., Gao, S., Yan, H., Sun, Z., Lian, Z., Duanmu, L., Zhang, Y., Zhou, X., et al. (2024). Comparative analysis of indoor thermal environment characteristics and occupants' adaptability: Insights from ASHRAE RP-884 and the Chinese thermal comfort database. Energy Build. *309*, 114033. https://doi.org/10.1016/j.enbuild.2024.114033.
44. Zhou, J., Chen, T.G., Tsurimaki, Y., Hajj-Ahmad, A., Fan, L., Peng, Y., Xu, R., Wu, Y., Assawaworrarit, S., Fan, S., et al. (2023). Angle-selective thermal emitter for directional radiative cooling and heating. Joule *7*, 2830–2844. https://doi.org/10.1016/j.joule.2023.10.013.
45. Zhao, W., Zhang, H., Zheng, J., Dai, Y., Huang, L., Shang, W., and Liang, Y. (2021). A point prediction method based automatic machine learning for day-ahead power output of multi-region photovoltaic plants. Energy *223*, 120026. https://doi.org/10.1016/j.energy.2021.120026.
46. An, J., Yan, D., Guo, S., Gao, Y., Peng, J., and Hong, T. (2020). An improved method for direct incident solar radiation calculation from hourly solar insolation data in building energy simulation. Energy Build. *227*, 110425. https://doi.org/10.1016/j.enbuild.2020.110425.
47. Varshney, A.K., Muhuri, P.K., and Lohani, Q.M.D. (2022). PIFHC: The Probabilistic Intuitionistic Fuzzy Hierarchical Clustering Algorithm. Appl. Soft Comput. *120*, 108584. https://doi.org/10.1016/j.asoc.2022.108584.
48. Chen, X., and Yang, X. (2021). Solar collector with asymmetric compound parabolic concentrator for winter energy harvesting and summer overheating reduction: Concept and prototype device. Renew. Energy *173*, 92–104. https://doi.org/10.1016/j.renene.2021.03.119.
49. Duffie, J.A., and Beckman, W.A. (2013). Solar Engineering of Thermal Processes, fourth ed. (John Wiley & Sons, Inc.).
50. Widyolar, B., Jiang, L., Ferry, J., and Winston, R. (2018). Non-tracking East-West XCPC solar thermal collector for 200 celsius applications. Appl. Energy *216*, 521–533. https://doi.org/10.1016/j.apenergy.2018.02.031.
51. Nadeem, A., Sher, H.A., Murtaza, A.F., and Ahmed, N. (2021). Online current-sensorless estimator for PV open circuit voltage and short circuit current. Sol. Energy *213*, 198–210. https://doi.org/10.1016/j.solener.2020.11.004.
52. Sun, Y. (2018). Research on model and parameter identification. Master's Thesis (South China University of Technology).
53. Yadav, V.K., Yadav, A., Yadav, R., Mittal, A., Wazir, N.H., Gupta, S., Pachauri, R.K., and Ghosh, S. (2022). A novel reconfiguration technique for improvement of PV reliability. Renew. Energy *182*, 508–520. https://doi.org/10.1016/j.renene.2021.10.043.
54. Barrientos-Espillco, F., Gascó, E., López-González, C.I., Gómez-Silva, M.J., and Pajares, G. (2023). Semantic segmentation based on Deep learning for the detection of Cyanobacterial Harmful Algal Blooms (CyanoHABs) using synthetic images. Appl. Soft Comput. *141*, 110315. https://doi.org/10.1016/j.asoc.2023.110315.

STAR★METHODS

KEY RESOURCES TABLE

REAGENT or RESOURCE	SOURCE	IDENTIFIER
Software and algorithms		
Matlab Vision 2021	The MathWorks, Inc	https://matlab.mathworks.com/
Python Vision 3.6	Python Software Foundation	https://www.python.org/
DeST Vision 20230713	Tsinghua University	Update.dest.net.cn
Arcgis Pro	Esri company	https://www.esri.com/en-us/arcgis/products/arcgis-pro/overview
U-net	Sun et al.[42]	https://doi.org/10.1016/j.apenergy.2022.119025
Other		
Algorithm for calculating indoor temperature of photovoltaic heating with building envelope thermal storage	This paper	N/A

RESOURCE AVAILABILITY

Lead contact

Further information and requests for resources and reagents should be directed to and will be fulfilled by the lead contact, Yuan Zhi (zhiy21@mails.tsinghua.edu.cn).

Materials availability

This study did not generate new unique reagents.

Data and code availability

- Data reported in this paper will be shared by the lead contact upon request.
- All original code is available in this paper's supplemental information.
- Any additional information required to reanalyze the data reported in this paper is available from the lead contact upon request.

EXPERIMENTAL MODEL AND STUDY PARTICIPANT DETAILS

In this study, the thermal model of the building-envelope-based PV heating system has two components. The first part of the model is the charging model of the thermal battery, which calculated the time-by-time power of the PV system. The PV power calculation includes the prediction of meteorological parameters based on hierarchical clustering, irradiance calculation based on coordinate analysis, and the MPPT algorithm.[38] Another part of the model is the exothermic modeling of the thermal battery, which is the calculation of the building heating load based on heat storage in the envelope. The heating line inside the thermal storage wall was defined as a thermal disturbance, the value of which was calculated using the PV power model. The heating load of the building was calculated based on different methods using the building energy consumption software DeST.[39–41] The model can be adapted to different climate types and weather conditions, and DeST can be used to model buildings with different structures.

Thermal battery charging model

Meteorological parameter prediction

PV power is closely related to weather conditions, and irradiance and temperature are essential parameters affecting the generating capacity of PV panels.[45] Therefore, obtaining future weather conditions in advance is necessary for predicting PV power. In this study, a hierarchical clustering method is proposed to achieve rapid hourly irradiance prediction.

The core of the cluster analysis involves dividing points at different positions into different types according to their similarity in the distance. The bottom-up clustering method was adopted; that is, points with similar distances formed a cluster, clusters with similar distances formed a group, and finally, the method formed a cluster tree from the bottom up. In this study, the historical hourly irradiance, including direct, total, and diffusion irradiance, was exported from the PV calculation software PVSYST[46] and divided into four seasons: spring, summer, fall, and winter. According to the weather type standard formulated by the Meteorological Administration, the weather conditions were divided into 34 types. Because similar weather types have similar irradiance characteristics in Ruicheng County (north latitude 34°36′-48,′ east longitude 110°36′-42′), China, in this study, five types of generalized weather, which involve the most common weather conditions based on

historical meteorological data, were considered. The hourly daily radiation of each season was grouped into five categories representing the five weather conditions: sunny, rainy, cloudy, sunny to cloudy, and cloudy to sunny. Each weather condition in each season corresponds to a specific hourly irradiance.

The calculation procedure for the hierarchical clustering algorithm comprises seven steps (Figure S1). In Steps 1 to 3, the input dataset and number of clusters were provided. In Step 4, the membership function μ and the non-membership function ν can be defined as[47]

$$\mu_i = \frac{x_i - x_{min}}{x_{max} - x_{min}} \quad \text{(Equation 2)}$$

then

$$\nu_i = \left[1 - \left(\frac{x_i - x_{min}}{x_{max} - x_{min}}\right)^{\kappa}\right]^{\frac{1}{\kappa}} \quad \text{(Equation 3)}$$

where x_i is an element of the hourly irradiance matrix, which is defined as

$$\psi = 1 - \nu - \mu \quad \text{(Equation 4)}$$

where $\mu \in (0,1)$, $\nu \in (0,1)$, and $0 \leq \mu_i + \nu_i \leq 1$. The correlation coefficient ω, which acts as the weight for the hesitance component, is computed as follows:

$$\omega(A,B) = 1 - \frac{1}{n}\sum_{i=1}^{n}\frac{\sigma_i}{1+\sigma_i} \quad \text{(Equation 5)}$$

where A and B represent two matrices: $\sigma_i = |\mu_A(x_i) - \mu_B(x_i)| + |\nu_A(x_i) - \nu_B(x_i)| + |\psi_A(x_i) - \psi_B(x_i)|$. After computing the weights for all matrices, we can compute the probabilistic Euclidean distances between each pair of data points and store them in a matrix, for example, a distance matrix, whose size is 1 × 24. Using the weights obtained from Equations 2, 3, 4, and 5 for the membership, non-membership, hesitance degree, and hesitation components, respectively, the distance between the matrices can be expressed as follows:

$$d(A,B) = \left\{\frac{1}{2n}\sum_{i=1}^{n}\left[(\mu_A(x_i) - \mu_B(x_i))^2 + (\nu_A(x_i) - \nu_B(x_i))^2 + \omega(A,B)(\psi_A(x_i) - \psi_B(x_i))\right]\right\}^{\frac{1}{2}} \quad \text{(Equation 6)}$$

In this equation, we consider each pair of data points as an individual cluster in Step 4, and enter the loop in Step 5.

In Step 6, we check the number of clusters for the termination condition. If the required number of clusters is obtained, the loop is terminated. Because the number of rows in the distance matrix represents the number of clusters formed in the algorithm, we can check for the termination condition as follows. If the number of rows (size (dist, 1)) in the distance matrix is greater than the number of given clusters (c), we proceed to Step 7; otherwise, we terminate the loop and reach the end of the algorithm.

In Step 7, after computing the distance matrix for each pair of data points, the minimum distance pair is selected and merged to form a cluster. The minimum-distance pair is the closest pair of clusters. After the minimum distance pair is merged, the distance matrix is updated, whereby each pair of data points is considered as an individual cluster. With each iteration, the minimum distant pair cluster in the distance matrix is merged, and the distance matrix for the merged cluster and other clusters is updated.

Taking the historical meteorological data of Ruicheng County, Shanxi Province, Central China, in winter as an example, matrices of total radiation corresponding to each weather condition were obtained, and the cluster analysis results are shown in Figure S3.

Thus, the corresponding hourly direct irradiance and diffusion irradiance can be obtained according to the weather conditions provided by the Meteorological Administration. The predicted future hourly temperature change was also obtained directly from the Meteorological Administration website so that the hourly meteorological parameters affecting the PV power in the future could be obtained using the hierarchical clustering method. For weather conditions with turning points, qualified hourly irradiance parameters were selected according to the turning points provided by the meteorological network.

Prediction of receiving radiation

To obtain the actual irradiance received by the PV panels, the proportion of direct radiation received by the PV panels was calculated according to the relative positions of the sun and the PV panels, and the proportion of sky diffusion and ground reflection received by the PV panels was determined according to the inclinations of the PV panels. The sum of the irradiances of these parts was the radiation received by the PV panel surface.

First, a three-dimensional Cartesian coordinate system was established with three axes pointing perpendicular to the ground: due south and due east. Next, the positional relationship between the sun and the photovoltaic panel was described in this coordinate system. Figure 4 illustrates the relationship between the solar position and the collectible solar irradiation for the photovoltaic panel. The incoming beam radiation can be divided into two perpendicular components. One component was the portion of the radiation projected onto the N–S vertical plane (Figure S4). The other component was parallel to the horizontal plane. The latter component does not contribute to the radiation available to the photovoltaic panel, and can be neglected.

The position of the sun can be expressed as[48]

$$\begin{aligned} S1 &= \cos\delta\cdot\cos\varphi\cdot\cos\varsigma+\sin\delta\cdot\sin\varphi \\ S2 &= -\cos\delta\cdot\sin\varsigma \\ S3 &= \cos\delta\cdot\sin\varphi\cdot\cos\varsigma-\sin\delta\cdot\cos\varphi \end{aligned} \quad \text{(Equation 7)}$$

where ζ is the solar hour angle; $\varnothing$ is the latitude, i.e., the angular location north or south of the equator; δ is the declination, i.e., the angular position of the sun at solar noon (i.e., when the sun is on the local meridian) with respect to the plane of the equator, where north is positive; and the declination can be expressed as[49]

$$\begin{aligned} \delta = \frac{180}{\pi}(&0.006918-0.399912\cos B+0.070257\sin B-0.006758\cos 2B+0.000907\sin 2B \\ &-0.002697\cos 3B+0.00148\sin 3B) \end{aligned} \quad \text{(Equation 8)}$$

where B can be expressed as

$$B = (n-1)\cdot\frac{360}{365} \quad \text{(Equation 9)}$$

where n is the nth day of the year. The solar hour angle can be expressed as[50]

$$\begin{aligned} \varsigma &= \frac{180}{\pi}(\omega-12)\cdot 15 \\ \omega &= t+4(L_{st}-L_{loc})+E \end{aligned} \quad \text{(Equation 10)}$$

where L_{st} is the standard meridian for the local time zone, L_{loc} is the longitude of the location in question, and the longitudes are in degrees west; ω is the time based on the apparent angular motion of the sun across the sky with solar noon being the time the sun crosses the meridian of the observer; and E is a time-dependent coefficient, which can be expressed by

$$E = 229.2\cdot\begin{pmatrix} 0.000075+0.001868\cos B-0.032077\sin B \\ -0.014615\cos 2B-0.04089\sin 2B \end{pmatrix} \quad \text{(Equation 11)}$$

The unit normal vector coordinates of the photovoltaic panels can be expressed by

$$V_p = (\cos\beta, 0, \sin\beta) \quad \text{(Equation 12)}$$

where V_p are the unit normal vector coordinates of the photovoltaic panels, β is the angle between the photovoltaic panel and the horizontal plane, and the angle between the direct radiation emitted by the sun and the normal line of the photovoltaic panel can be expressed as

$$\theta_p = \frac{180}{\pi}\cdot\arccos(V_p\cdot V_s) \quad \text{(Equation 13)}$$

where θ_P is the included angle between the direct radiation emitted by the sun and the normal line of the photovoltaic panel, and V_s is the coordinate of the position of the sun, which is (S1, S2, S3).

The solar radiation received on the surface of the photovoltaic panels is composed of three parts: direct irradiance, sky diffusion irradiance, and ground reflection irradiance. The direct irradiance can be expressed as

$$G_z = DNI\cdot\cos\theta_p \quad \text{(Equation 14)}$$

where G_z is the direct irradiance photovoltaic panel (W/) and DNI is the hourly direct irradiance obtained by hierarchical clustering (W/) m^2. Sky diffusion radiation can be expressed as

$$G_s = I_k\cdot\frac{1+\cos\beta}{2} \quad \text{(Equation 15)}$$

where G_s is the sky diffusion irradiance received by the photovoltaic panels (W/) m^2, and I_k is the hourly diffusion irradiance obtained by hierarchical clustering (W/) m^2. The ground reflection irradiance can be expressed as

$$G_f = I_g\cdot\rho\frac{1-\cos\beta}{2} \quad \text{(Equation 16)}$$

where G_f is the ground reflection irradiance received by the photovoltaic panel (W/m^2) and I_g is the hourly total irradiance obtained by hierarchical clustering (W/m^2). The total hourly solar irradiance received on the surface of photovoltaic panels is given by

$$G_t = G_z+G_s+G_f \quad \text{(Equation 17)}$$

Equivalent circuit model

The equivalent circuit model for photovoltaic panels under standard conditions is shown as[51]

$$I_{sc} = \left[1 - P_1\left(e^{\frac{U}{P_2 U_{oc}}} - 1\right)\right]$$
$$P_1 = \left(1 - \frac{I_m}{I_{sc}}\right) e^{-\frac{U_m}{P_2 U_{oc}}} \quad \text{(Equation 18)}$$
$$P_2 = \left(\frac{U_m}{U_{oc}} - 1\right)\left[\ln\left(1 - \frac{I_m}{I_{sc}}\right)\right]^{-1}$$

where I_{sc} is the short-circuit current, A; I_m is the current at the maximum power point, A; U_m is the voltage at the maximum power point, V; U_{oc} is the open-circuit voltage, V; and Equation 18 is only applicable under standard test conditions, that is, a total irradiance of 1000W/m^2 and a temperature of 25°C. However, in practical engineering, the temperature and irradiance differ; therefore, the parameters in Equation 18 must be modified, as shown[52]

$$I_{sc} = I_{sc\_ref}\frac{G_t}{G_{ref}}(1 + \alpha\Delta T)$$
$$U_{oc} = U_{oc\_ref}\ln(e + b\Delta G)(1 - c\Delta T) \quad \text{(Equation 19)}$$
$$I_m = I_{m\_ref}\frac{G_t}{G_{ref}}(1 + \alpha\Delta T)$$
$$U_m = U_{m\_ref}\ln(e + b\Delta G)(1 - c\Delta T)$$

where α, b, and c are compensation coefficients for the temperature and irradiance. The values of these three numbers are 00025 (°C)$^{-1}$, 0.0005 (W/m^2)$^{-1}$, and 0.00288 (°C)$^{-1}$, respectively, according to a large amount of experimental data [9-11]. I_{sc_ref} is the short-circuit current under standard test conditions, A; I_{m_ref} is the current at the maximum power point under standard test conditions, A; U_{m_ref} is the voltage at the maximum power point under standard test conditions, V; U_{oc_ref} is the open-circuit voltage under standard test conditions, V; G_{ref} is the standard total irradiance, 1000w/m^2; and ΔT is the difference between the actual temperature and the standard temperature, °C.

Improved MPPT algorithm

The volt-ampere characteristics of photovoltaic panels can be obtained through the diode model, but different output voltages of PV panels will lead to different output powers; thus, the actual output power of the photovoltaic panels remains unknown. In an actual project, a converter with the MPPT algorithm is installed between the photovoltaic panel and the load side to ensure that the photovoltaic panel generates power at the parameter point with maximum power on the U-I diagram. Therefore, the MPPT algorithm was added to the photovoltaic power prediction model. In this study, the modified conductance increment method was used to determine the power point of the photovoltaic panels.

In the U-I image of the photovoltaic circuit, the partial derivative of the maximum power point with respect to the voltage is zero, as shown in[53]

$$\frac{dP}{dU} = \frac{d(IU)}{dU} = U\frac{dI}{dU} + I = 0 \quad \text{(Equation 20)}$$

Equation 21 defines an index K, and the distance from the maximum power point and the adjustment direction can be determined using the value of K in the calculation process.

$$K = \frac{dI}{dU} + \frac{I}{U} \quad \text{(Equation 21)}$$

When $K > 0$, the output voltage must be increased to the left of the maximum power point to reach the maximum power point; when $K < 0$, the output voltage must be decreased to the right of the maximum power point to reach the maximum power point; and when $K = 0$, the output power is directly at this point without adjustments to the voltage.

However, the traditional conductance increment method requires a long convergence time because of the random selection of the initial point. Therefore, in combination with the idea of the constant voltage method, the initial point is set to 0.7 U_m in this study, which can reduce the convergence time and response time compared with the traditional random selection method. The voltage step is lower than the traditional value, which can increase the adjustment accuracy and avoid back and forth oscillations at the maximum power point. The principle of the improved conductance increment method is shown in Figure S5.

Exothermic modeling of the thermal battery

The model establishes heat transfer equations for the envelope structure of the room and the air in the room, considers the PV power as a thermal disturbance, and then solves it based on the difference method.

First, the heat transfer equation for the wall was established. Considering the north wall as an example, the heat conduction equation for this wall is expressed as follows:

$$\rho_w c_w \frac{\partial t_w}{\partial \tau} = \lambda_w \frac{\partial^2 t_w}{\partial x^2} \quad \text{(Equation 22)}$$

where, ρ_w is the density of the wall, kg/m^3; c_w is the specific heat capacity of the wall, J/(kg*°C); λ_w is the thermal conductivity of the wall, W/(m*°C); t_w is the temperature of the wall, °C. The north wall is divided into n layers along the thickness direction, where the thickness of the layer in contact with the indoor air and outdoor air is d/2, and the distance between the nodes in the middle is d. Therefore, for the outermost layer of the north wall, that is, the node with n=1, the heat transfer equation is given by

$$\frac{d}{2}\rho_w c_w \frac{\partial t_{w,1}}{\partial \tau} = \frac{2\lambda_w}{d}(t_{w,2} - t_{w,1}) + h_o(t_o - t_{w,1}) \quad \text{(Equation 23)}$$

where, h_o is the convective heat transfer coefficient between the outdoor air and the outer surface of the north wall, W/(m^{2*}°C) and t_o is the temperature of the outdoor air, °C.

For the layer in the middle of the north wall, that is, the node between 1-n+1, the heat transfer equation is given by

$$d\rho_w c_w \frac{\partial t_{w,i}}{\partial \tau} = \frac{\lambda_w}{d}(t_{w,i-1} - t_{w,i}) + \frac{\lambda_w}{d}(t_{w,i+1} - t_{w,i}) \quad \text{(Equation 24)}$$

For the innermost layer of the north wall, when the number of nodes is n+1, the heat transfer equation is as follows:

$$\frac{d}{2}\rho_w c_w \frac{\partial t_{w,n+1}}{\partial \tau} = \frac{2\lambda_w}{d}(t_{w,n} - t_{w,n+1}) + h_{in}(t_a - t_{w,n+1}) + h_f(t_f - t_{w,n+1}) + \sum_{i=1}^{4} h_{r,i}(t_{r,n+1} - t_{w,n+1}) \quad \text{(Equation 25)}$$

where, h_{in} is the convective heat transfer coefficient between the indoor air and the inter surface of the north wall, W/(m^{2*}°C); t_a is the temperature of the indoor air, °C; h_r is the convective heat transfer coefficient of the equivalent to the radiation between the inter surface of the other walls and the inner surface of the north wall, W/(m^{2*}°C), this item represents the radiant heat exchange between the north wall and the other walls and roofs; h_f is the convective heat transfer coefficient of the equivalent to the radiation between the surface of the floor and the inter surface of the north wall, W/(m^{2*}°C), this item represents the radiant heat exchange between the north wall and the floor; t_f is the temperature of the surface of the floor, °C; $t_{r,n+1}$ is the temperature of the surface of the other walls and the roof, °C;

The floor is assumed to be adiabatic, and the heat transfer equation for the floor is given by

$$h_{fa}(t_a - t_f) + \sum_{i=1}^{5} h_{fr,i}(t_{r,n+1} - t_f) = 0 \quad \text{(Equation 26)}$$

where, h_{fa} is the convective heat transfer coefficient between the indoor air and the surface of the floor, W/(m^{2*}°C); h_{fr} is the convective heat transfer coefficient of the equivalent to the radiation between the surface of the floor and the surface of the other walls, W/(m^{2*}°C), this item represents the radiant heat exchange between the floor and the other walls and roofs. Equation 26 gives an analytical solution for the floor temperature, $t_f = \frac{h_{fa}t_a + \sum_{i=1}^{5} h_{fr}t_{r,n+1}}{h_{fa} + \sum_{n=1}^{5} h_{fr}}$.

Similar to the heat transfer calculation process for the wall, the glass of the window was divided into three layers along the thickness direction, and the heat transfer equation of the outermost layer is as follows:

$$d_{win}\rho_{win}c_{win}\frac{\partial t_{win,1}}{\partial \tau} = \frac{\lambda_{win}}{d_{win}}(t_{win,2} - t_{win,1}) + h_{wo}(t_o - t_{win,1}) \quad \text{(Equation 27)}$$

where, ρ_{win} is the density of the window, kg/m^3; c_{win} is the specific heat capacity of the window, J/(kg*°C); λ_{win} is the thermal conductivity of the window, W/(m*°C); t_{win} is the temperature of the window, °C. h_{wo} is the convective heat transfer coefficient between the outdoor air and the outer surface of the window, W/(m^{2*}°C);

For the layer in the middle of the window, the heat transfer equation is as follows:

$$d_{win}\rho_{win}c_{win}\frac{\partial t_{win,2}}{\partial \tau} = \frac{\lambda_{win}}{d_{win}}(t_{win,1} - t_{win,2}) + \frac{\lambda_{win}}{d_{win}}(t_{win,3} - t_{win,2}) \quad \text{(Equation 28)}$$

For the innermost layer of the window, the heat transfer equation is shown as

$$d_{win}\rho_{win}c_{win}\frac{\partial t_{win,3}}{\partial \tau} = \frac{\lambda_{win}}{d_{win}}(t_{win,2} - t_{win,3}) + h_{win}(t_a - t_{win,3}) + h_{wf}(t_f - t_{win,3}) + \sum_{i=1}^{4} h_{wr,i}(t_{wr,n+1} - t_{win,3}) \quad \text{(Equation 29)}$$

where, h_{win} is the convective heat transfer coefficient between the indoor air and the inter surface of the window, W/(m^{2*}°C); h_{wr} is the convective heat transfer coefficient of the equivalent to the radiation between the inter surface of other walls and the inter surface of the window, W/(m^{2*}°C), this item represents the radiant heat exchange between the window and the other walls and roof; h_{wf} is the convective heat transfer

coefficient of the equivalent to the radiation between the surface of the floor and the inter surface of the window, W/(m^2*°C), this item represents the radiant heat exchange between the window and the floor; $t_{wr,n+1}$ is the temperature of the surface of the roof, the other walls and the roof, °C.

The heat transfer equation for the indoor air node is as follows:

$$\rho_a c_a V \frac{\partial t_a}{\partial \tau} = \sum_{i=1}^{5} F_w h_{r,i}(t_{w,i+1} - t_a) + q_v + q_s + F_f h_{fa}(t_f - t_a) + F_{win} h_{win}(t_{win,3} - t_a) \quad \text{(Equation 30)}$$

where, ρ_a is the density of the air, kg/m^3; c_a is the specific heat capacity of the air, J/(kg*°C); F_w is the area of the wall, m^2; F_{win} is the area of the window, m^2; F_f is the area of the floor, m^2; q_v is the heat loss of ventilation, W; q_s is the heat gain in the room, W.

Simultaneously, with the above heat transfer equations, the heat balance equation for the entire room is established as follows:

$$C\dot{T} = AT + Bu \quad \text{(Equation 31)}$$

where C represents the heat capacity; A represents the relationship between each temperature node; B represents the contribution of each thermal disturbance to the temperature node; and u represents each thermal disturbance term, including the matrices of ventilation, indoor heat gain, and outdoor temperature.

U-net convolutional neural network model

In this study, the semantic segmentation model U-net algorithm was used to analyze satellite images of all Chinese cities to obtain the roof area of each city and calculate the building PV installation potential.[42] Original satellite image data were obtained from Google Maps, and the images were segmented into 256×256 pixels using the remote sensing software ArcGIS. The segmented images were then flipped, mirrored, and enhanced to form the training set for the U-net model. In the U-net model, the size of the satellite images was continuously reduced from 256×256 to 128×128, 64×64, 32×32, and 16×16 px. Simultaneously, the feature channels were multiplied in each transformation step to 1024. Finally, an upward convolution was applied to double the resolution of the feature map and halve the number of channels. Subsequently, feature maps from the same layer of the left shrinkage path were concatenated, and two 3 × 3 convolutions and ReLU were applied. This was repeated on the right path until the resolution of the feature maps matched that of the input images.[54] Once the model had been trained, it was applied in a test set that cut city-level satellite imagery across the country to obtain the national building rooftop areas and PV installation potential.

To train this model, we used the SoftMax function to calculate the classification probability of each pixel in the last layer and used the cross-entropy loss function as the target. Gradient optimization was performed according to the Adam algorithm, as shown in Equations 32 and 33, as follows.

$$p_n(x) = exp(a_n(x)) \Big/ \left(\sum_{n}^{N} exp(a_{k(x)}) \right) \quad \text{(Equation 32)}$$

$$E = \sum_{x \in \Omega} w(x) \log\left(p_{l(x)}(x)\right) \quad \text{(Equation 33)}$$

where $a_n(x)$ denotes the activation in the feature channel n at pixel position $x \in \Omega$ with $\Omega \in Z^2$, N is the number of classes, and $P_N(x)$ is the approximated maximum function. Ω is the true label of each pixel and w is a weight map that we used to give some pixels more importance in the training process.

The building PV potential was obtained by multiplying the local irradiance with the roof area, PV generation efficiency, and shading factor. The irradiance of each area was obtained using the PVsyst software. The shading factor of the PV is taken as 0.4 for urban buildings and 0.6 for rural buildings.

METHOD DETAILS

Material characterization

The diameter of the carbon-fiber electric wire was 5.5 mm, and the thickness of each layer was 1 mm. The resistance of the carbon fiber is 16.8 ohms per meter. SEM images were acquired using an FEI Nova NanoSEM instrument (5 kV).

Thermal measurements

We conducted experiments in Ruicheng County, central China. The outdoor irradiance and temperature in Ruicheng County are shown in Figure S7 in the supplemental information. The heating area of the room was 15 m^2, the installed PV capacity was 5.3 kW, and the heat-storage wall area was 13 m^2. We arranged temperature sensors in the farmhouse and collected test data over the entire heating season, from November 2021 to March 2022. The physical parameters tested include the indoor air temperature, outdoor air temperature, indoor black bulb temperature, heat storage wall surface temperature, heating wire surface temperature, temperature at the center of the thermal storage wall, and temperature on the surface of the insulation board. The temperature sensor has an accuracy of 0.1°C and a range of -30°C to 100°C.